Flexibility of the quasi-non-uniform exchange-correlation approximation

H. Levämäki,* M. P. J. Punkkinen, and K. Kokko
Department of Physics and Astronomy, University of Turku, FI-20014 Turku, Finland
and Turku University Centre for Materials and Surfaces (MatSurf), Turku, Finland

L. Vitos†
Applied Materials Physics, Department of Materials Science and Engineering, Royal Institute of Technology, Stockholm SE-100 44, Sweden;
Department of Physics and Astronomy, Division of Materials Theory, Uppsala University, Box 516, SE-75121, Uppsala, Sweden;
and Wigner Research Centre for Physics, Institute for Solid State Physics and Optics, H-1525 Budapest, P.O. Box 49, Hungary
(Received 24 January 2014; published 5 March 2014)

In our previous study [Phys. Rev. B **86**, 201104 (2012).] we introduced the so-called quasi-non-uniform gradient-level exchange-correlation approximation (QNA) and demonstrated its strength in producing highly accurate equilibrium volumes for metals and their alloys within density-functional theory. In this paper we extend the scheme to include the accuracy of the bulk modulus as an additional figure of merit and show that this scheme is flexible enough to allow the computation of accurate equilibrium volumes and bulk moduli at the same time. The power and feasibility of this scheme is demonstrated on NiAl and FeV binary alloys.

DOI: 10.1103/PhysRevB.89.115107 PACS number(s): 71.15.Mb, 71.15.Nc, 64.30.Ef, 71.20.Be

I. INTRODUCTION

Density-functional theory [1,2] has become the most widely used method in determining the electronic properties of atoms, molecules and solids. It's success stems from the surprising accuracy of the earliest exchange-correlation (xc) approximation, the local-density approximation (LDA) [2]. Going beyond LDA within the framework of the local density formalism leads to gradient-level density functionals (GDFs), which can be divided into two main families. The generalized gradient approximation [3] (GGA) managed to stabilize the diverging term in the second-order gradient expansion [2] and gave, e.g., a qualitatively correct description for the ground state of ferromagnetic iron [4–6]. The subsystem functional approach (SFA) [7] originates from the nearsightedness principle [8] and incorporates inhomogeneous electron density effects through well-adapted model systems. For both GDF families, LDA represents the lowest-order approximation and thus the correct limit in systems with densities showing negligible inhomogeneities. LDA together with the Perdew–Burke–Ernzerhof (PBE) [9] GGA are the two most widely used xc functionals for condensed matter.

In DFT, assuming proper numerical implementation of the software, the accuracy of the results for well-converged calculations depends only on the chosen xc functional. However, there is no functional that could provide systematic accuracy for a wide range of solids. In our previous work [10] we introduced the concept of quasi-non-uniform gradient-level xc approximation (QNA) and showed that it is able to produce highly accurate equilibrium volumes for metals and their alloys. This scheme is based on the observation that, for metals, the beyond-LDA features of a GGA-type xc functional only matter in the valence-core overlap regions centered around the atomic sites. The error of a GDF is thus mainly local in nature. This finding concurs with the discussions in Refs. [11–13] and it allows one to define a new SFA in which each (element-specific) valence-core overlap region constitutes a subsystem and these subsystems are connected by the nearly homogeneous, LDA-like valence-electron sea. For a general multicomponent system then, one can apply local corrections in each core-valence overlap region separately and the overall QNA functional can mathematically be expressed as a superposition of the subsystem functionals, viz.

$$E_{\rm xc}^{\rm QNA}[n] = \sum_q \int_{\omega_q} \epsilon_{\rm x}^{\rm LDA}(n) F_{\rm xc}^{{\rm opt}_q}(r_s,s) d^3r, \qquad (1)$$

where $r_s = [3/(4\pi n)]^{1/3}$, $s = |\nabla n|/[2n(3\pi^2 n)^{1/3}]$, and $F_{\rm xc}^{{\rm opt}_q}$ in this case (see next paragraph) is the GGA enhancement function of the subsystem functional for the alloy component q. Around each atomic site q, the integration domain is within ω_q. These space-filling polyhedra ω_q are defined so that the gradient of the density (and thus s) vanishes on the boundary of each ω_q.

Defining the optimal subsystem functionals could be done in different ways. In this work we use perhaps the simplest procedure. Namely, all subsystem functionals have the same analytical form and only some "tunable" parameters are changed. Thus, for each element so-called "optimal" parameters have to be found. In our previous work (see Ref. [10]) these optimal parameters were chosen in such a way that the error in equilibrium volume vanished. In this paper we extend our scope and investigate how well this process can be done when the error in equilibrium volume (V_0) and bulk modulus (B_0) are both taken into account. To this end, for each element we find such optimal parameters that minimize the objective function that we have chosen to be the combined absolute relative error:

$$f(^*{\rm args}) = {\rm W_a}\frac{|{\rm a_0}(^*{\rm args}) - {\rm a_{expt}}|}{\rm a_{expt}} + {\rm W_B}\frac{|{\rm B_0}(^*{\rm args}) - {\rm B_{expt}}|}{\rm B_{expt}}, \qquad (2)$$

where a is the lattice constant, B is the bulk modulus, expt signifies experimental values and *args represents the tunable

*hpleva@utu.fi
†levente@kth.se

parameters that the functional form in use has. W_a and W_B are weights that can be chosen appropriately. We have chosen to use the framework of PBE and PBEsol [14] due to its simple yet powerful construction. PBE was designed to provide accurate atomic energies whereas PBEsol was optimized for bulk and surface systems by restoring the original gradient expansion behavior for the exchange part and adjusting the correlation term using the jellium surface exchange-correlation energies obtained at meta-GGA level. Both PBE and PBEsol have two parameters, μ and β, which control the strength of exchange (μ) and correlation (β) corrections over LDA. Their PBE and PBEsol values are $(\mu,\beta)_{\mathrm{PBE}} = (0.219\,515, 0.066\,725)$ and $(\mu,\beta)_{\mathrm{PBEsol}} = (0.123\,457, 0.046\,000)$, respectively. Finding optimal parameters, which is to say minimizing Eq. (2), thus in this case becomes a two-dimensional optimization problem. In this work such optimization for 25 elements has been done. This group contains 10 cubic sp metals and 15 transition metals.

II. COMPUTATIONAL METHOD

The electronic structure and total-energy calculations from which the optimal parameters were derived were performed employing the exact muffin-tin orbitals (EMTO) method [15–17]. Gradient corrections have been taken into account in a non-self-consistent (NSC) manner, which is to say self-consistent (SC) calculations were carried out within LDA and the gradient terms were included in the total energy within the perturbative approach [18]. The reason behind favoring the NSC approach in this case is that it greatly reduces the required computational time. This way the resource-intensive self-consistent Kohn-Sham loops can be completed first so that the optimization process only involves fast evaluations of the total energy. For Cr self-consistent GGA was employed instead of the perturbative approach. This is because, for antiferromagnetic Cr, the perturbative approach highly overestimates the bulk modulus and self-consistent GGA becomes necessary to correct for this error [19]. The Kohn-Sham equations were solved within the scalar relativistic approximation and the soft-core scheme. The Green's function was calculated for 16 complex energy points distributed exponentially on a semicircular contour including the valence states and employing the double Taylor expansion approach [20]. The EMTO basis set included s, p, d, and f orbitals ($l_{\max} = 3$), and in the one-center expansion of the full charge density $l^h_{\max} = 8$ was used. The amount of inequivalent $\vec{k}$ points was 27 434 and 28 884 in the irreducible wedge of the body-centered cubic (bcc) and face-centered cubic (fcc) Brillouin zones, respectively. The theoretical equilibrium lattice constants a_0 and bulk moduli B_0 were derived from the stabilized jellium equations of state (SJEOS) [21] fitted to the *ab initio* total energies calculated for 18 to 21 atomic volumes around the equilibrium. For each element Eq. (2) was minimized with weights $W_a = W_B = 1$ under the constraints of keeping the accuracy of the calculated Wigner–Seitz radius with respect to the experimental value roughly inside ± 0.005 Bohr and not letting β become greater than 0.1.

To assess the transferability of these NSC-derived optimal parameters into SC-GGA calculations additional SC-EMTO and FP − (L)APW + lo Elk [22] calculations have been carried out for Li, V, Fe, Cu, Nb, and Au. With Elk, a grid of $21 \times 21 \times 21$ $\vec{k}$ points (286 in the irreducible wedge) was used and $R^{\min}_{\mathrm{MT}} K_{\max}$, which determines the size of the basis set, was between 8 and 10. Spin-orbit coupling has been taken into account for Au. Lattice constants and bulk moduli were obtained from a SJEOS-fit to 10 to 11 points around the equilibrium.

Based on our experience the differences between NSC-EMTO and SC-EMTO results are expected to be quite small (see Sec. III C). However, problems in the SC-EMTO results may occur if the numerical derivatives of the density (especially with the second derivative) are not being calculated with sufficient accuracy. Even small deficiencies in the way the derivatives are calculated can be detrimental, because the error has a tendency to amplify itself after each iteration of the self-consistent Kohn-Sham loop.

III. RESULTS AND DISCUSSION

All experimental lattice constants and bulk moduli have either been reported at 0 K or extrapolated to 0 K using the linear thermal expansion coefficients α from Ref. [23]. Zero-point phonon effects (ZPPE) have also been subtracted out from both lattice constants and bulk moduli. For lattice constants, ZPPEs are in the form of a zero-point anharmonic expansion (ZPAE) and it can be estimated as explained in Refs. [21] and [24] by using the expression

$$\frac{\Delta a_0}{a_0} = \frac{1}{3}\frac{\Delta V_0}{V_0} = \frac{3}{16}(B_1 - 1)\frac{k_B \Theta_D}{B_0 V_{0,\mathrm{at}}}, \tag{3}$$

where $\Delta V_0/V_0$ is the fractional volume change caused by the inclusion of ZPAE leading to a correction Δa_0 to the experimental lattice parameter a_0. B_1 is the pressure derivative of the bulk modulus B_0, Θ_D is the Debye temperature (from Ref. [25]), and $V_{0,\mathrm{at}}$ is the experimental volume per atom. With bulk moduli, the ZPPEs have been taken into account using the procedure of Ref. [26], according to which

$$\Delta B_0 = B_1(P_t + P_z) = B_1\left(-\frac{\Delta V}{V}B - \frac{3}{16}B_1\frac{k_B\Theta_D}{B_0 V_{0,\mathrm{at}}}\right), \tag{4}$$

where $P_t = -B\Delta V/V$ is a small negative pressure associated with the thermal expansion of a material and P_z is the effective pressure required to mimic the effect of ZPPEs. In the present application, we used the data from Refs. [13] and [27] and the supplementary material from Ref. [28] to estimate B_1 from Eq. (3). For Cr, B_1 was estimated by using the data from Ref. [29]. The so-derived B_1 values were used in Eq. (4).

In this work a group of 25 metals is considered. This group contains monovalent sp metals (Li, Na, K, Rb, and Cs), cubic divalent sp metals (Ca, Sr, and Ba), Al, Pb, and cubid $3d$ (V, Cr, Fe, Ni, and Cu), $4d$ (Nb, Mo, Rh, Pd, and Ag), and $5d$ (Ta, W, Ir, Pt, and Au) metals. Experimental lattice constants are from Ref. [13] (Li, Na, K, Rb, Cs, Ca, Sr, Ba, Al, Pb, Cu, Rh, Pd, and Ag), Ref. [27] (V, Fe, Ni, Nb, Mo, Ta, W, Ir, Pt, and Au), and Ref. [23] (Cr). Experimental bulk moduli are from Ref. [13] (Li, Na, K, Rb, Cs, Ca, Sr, Ba, Al, Pb, Cu, Rh, Pd, and Ag), Ref. [30] (V), Ref. [25] (Cr, Ni, Nb, Mo, and Ir), Ref. [31] (Fe), and Ref. [32] (Ta, W, Pt, and Au).

TABLE I. Theoretical and experimental equilibrium lattice constants a_0 (in Å) and bulk moduli B_0 (in GPa) for the cubic sp, $3d$, $4d$, and $5d$ metals. Corresponding lattice structures are in parentheses. The experimental data have been corrected for temperature and ZPPE terms. Results are shown for PBE, PBEsol, and QNA functionals. The best theoretical values and statistical data are in boldface.

	a_0				B_0			
Solid	QNA	PBE	PBEsol	Expt.	QNA	PBE	PBEsol	Expt.
Li (bcc)	**3.444**	3.437	3.434	3.449	13.5	**13.9**	13.7	13.8
Na (bcc)	**4.204**	4.200	4.171	4.210	**7.55**	7.77	7.91	7.63
K (bcc)	**5.212**	5.286	5.214	5.212	**3.75**	3.58	**3.74**	3.75
Rb (bcc)	**5.581**	5.667	5.564	5.576	**2.95**	2.82	2.99	2.92
Cs (bcc)	**6.034**	6.167	6.016	6.039	**2.07**	1.96	2.03	2.11
Ca (fcc)	**5.546**	5.540	5.472	5.553	**17.9**	17.3	**17.9**	18.6
Sr (fcc)	**6.038**	6.031	5.933	6.045	**11.6**	**11.6**	13.4	12.5
Ba (bcc)	**4.991**	5.014	4.865	4.995	**8.33**	8.09	8.28	9.34
Al (fcc)	4.018	4.045	**4.019**	4.020	**80.8**	76.8	81.3	80.8
Pb (fcc)	**4.909**	5.053	4.947	4.902	48.3	39.3	**46.5**	47.0
V (bcc)	**3.024**	2.998	2.958	3.024	**163**	177	190	161
Cr (bcc)	**2.869**	**2.869**	2.808	2.877	**189**	184	252	194
Fe (bcc)	**2.854**	2.838	2.793	2.853	**175**	189	220	174
Ni (fcc)	**3.514**	3.526	3.470	3.508	200	**197**	228	195
Cu (fcc)	**3.602**	3.637	3.571	3.595	150	**139**	167	144
Nb (bcc)	**3.288**	3.310	3.269	3.294	167	162	**169**	174
Mo (bcc)	**3.137**	3.164	3.131	3.141	**266**	249	**266**	278
Rh (fcc)	3.800	3.846	**3.796**	3.793	**283**	251	288	271
Pd (fcc)	**3.882**	3.958	3.890	3.875	204	165	**201**	196
Ag (fcc)	**4.063**	4.163	4.068	4.056	119	88.0	**117**	110
Ta (bcc)	**3.295**	3.326	3.287	3.299	195	187	**196**	198
W (bcc)	3.165	3.191	**3.161**	3.160	**305**	293	311	300
Ir (fcc)	**3.838**	3.890	3.850	3.831	386	340	**377**	365
Pt (fcc)	**3.920**	3.988	3.936	3.913	**295**	242	282	289
Au (fcc)	**4.068**	4.176	4.101	4.062	186	135	**171**	178
ME[a] (Å$\times 10^{-2}$)	**0.06**	4.15	−2.23	ME (GPa)	**2.20**	−9.76	8.24	
MAE[b] (Å$\times 10^{-2}$)	**0.52**	4.95	3.52	MAE (GPa)	**4.62**	12.38	11.06	
MRE[c] (%)	**0.02**	0.95	−0.56	MRE (%)	**0.14**	−6.67	4.28	
MARE[d] (%)	**0.13**	1.17	0.87	MARE (%)	**3.32**	8.41	7.13	

[a]Mean error.
[b]Mean absolute error.
[c]Mean relative error.
[d]Mean absolute relative error.

Table I contains the calculated equilibrium lattice constants and bulk moduli for the 25 elements considered as well as the 0 K estimated experimental values. Results for PBE, PBEsol, and QNA functionals are included. Total mean error (ME), mean absolute error (MAE), mean relative error (MRE), and mean absolute relative error (MARE) for the lattice constants as well as the bulk moduli are also listed at the bottom of the table.

A. Lattice constants

The present trends for PBE and PBEsol are in line with investigations that have studied the performance of these functionals [13,27,33–36]. On average PBE tends to overestimate the volume while PBEsol does the opposite (see MEs and MREs in Table I). At least for the elements tested so far, it is always possible to find such optimal μ and β that the error in lattice constant vanishes. In fact, there is an infinite amount of such $\{\mu,\beta\}$ pairs forming a continuous curve in the $\{\mu,\beta\}$ space (see Fig. 1). If the accuracy of the bulk modulus was not to be taken into consideration QNA's MAE in Table I for lattice constants would consequently be zero. Even with the accuracy of the bulk modulus factored in, MAE of QNA is an order of magnitude smaller than those of PBE and PBEsol. In all but two cases QNA is able to produce the most accurate lattice constant, with the exceptions being Rh and W. For Rh and W, PBEsol already gives a very accurate lattice constant and some of this accuracy has been given up in QNA to better match the error in bulk modulus. The effect in both cases, however, remains rather modest; QNA lattice constant is only 0.004 Bohr larger that that of the best-performing functional.

It has been explained in Ref. [12] how the calculated equilibrium volume is determined by the slope $dE_{\rm xc}/dV$, where V is some measure for the volume. In this paper the Wigner–Seitz radius w will be used. Different slopes for different functionals arise from the core-valence overlap region with larger slopes corresponding to smaller volumes and vice versa. By changing the parameters μ and β one can manipulate the shape of the $F_{\rm xc}^{\rm opt_q}(r_s,s)$ map, which in turn

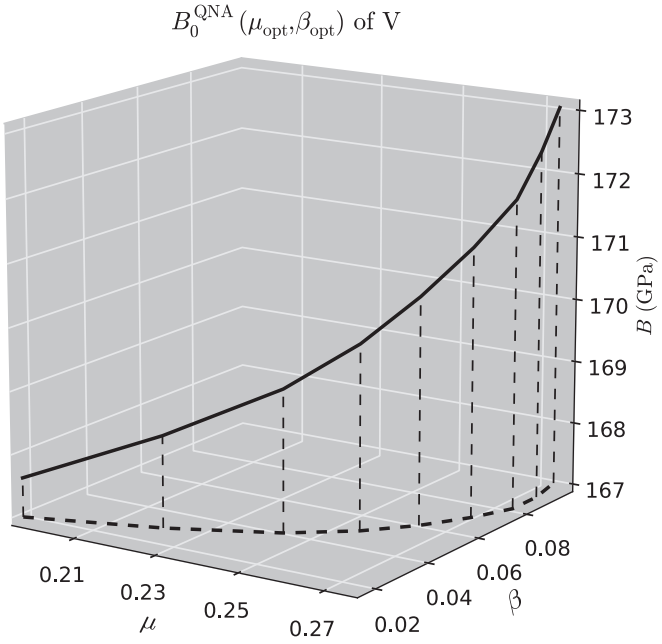

FIG. 1. QNA bulk modulus of V along the curve of such $\{\mu,\beta\}$ pairs, which all yield the same optimal volume (the thick dashed line).

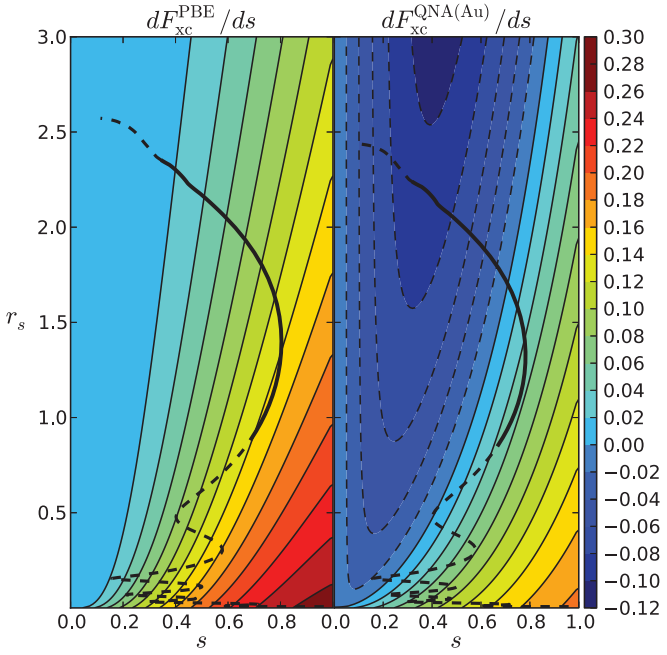

FIG. 2. (Color online) s-derivatives of the enhancement function F_{xc} for (left) PBE and (right) QNA(Au). The thick black lines represent the values of r_s and s of Au in the $\hat{z}$ direction within the Wigner–Seitz cell at the PBE and QNA equilibrium volumes. The solid portion of these lines represent the core-valence overlap region. Dashed contour lines represent negative regions.

is going to determine the slope dE_{xc}/dw. In the interesting region (core-valence overlap region) this slope is given by

$$\frac{\partial E_{\mathrm{xc}}^{\mathrm{cvor}}}{\partial w} = A(G_1 + G_2 + G_3), \tag{5}$$

where $A = (3/4)(3/\pi)^{1/3}[3/(4\pi)]^{4/3}$ and "cvor" stands for core-valence overlap region. The notation of Ref. [12] has been used, in which

$$G_1 = \int_{\mathrm{cvor}} \frac{4}{r_s^5}\frac{dr_s}{dw}F_{\mathrm{xc}}d^3r, \tag{6}$$

$$G_2 = -\int_{\mathrm{cvor}} \frac{1}{r_s^4}\frac{\partial F_{\mathrm{xc}}}{\partial r_s}\frac{dr_s}{dw}d^3r, \tag{7}$$

$$G_3 = -\int_{\mathrm{cvor}} \frac{1}{r_s^4}\frac{\partial F_{\mathrm{xc}}}{\partial s}\frac{ds}{dw}d^3r. \tag{8}$$

It is the interplay of G_1, G_2, and G_3 which determines the slope and as a result the lattice constant. G_1 is the strongest and positive, while G_2 and G_3 are generally one to two orders of magnitude weaker and negative in sign [12]. Note that for LDA G_3 is always zero since $\partial F_{\mathrm{xc}}/\partial s$ is zero by definition. For PBE, on the other hand, the $\partial F_{\mathrm{xc}}/\partial s$ term is always positive and relatively strong in the interesting region, as can be seen in Fig. 2. This figure also displays the parametric curves of r_s and s of Au in the $\hat{z}$ direction within the Wigner–Seitz cell at the PBE and QNA equilibrium volumes. The solid portions of these curves represent the core-valence overlap region and they illustrate what kind of $\partial F_{\mathrm{xc}}/\partial s$ values appear inside the integral of Eq. (8) for PBE and QNA. As a result, G_3^{PBE} cancels a fair amount out of G_1^{PBE}, leading to shallow slopes and overestimated lattice constants for many solids. But Au, for example, has optimal parameters $\mu = 0.125$ and $\beta = 0.1$ leading to a $\partial F_{\mathrm{xc}}/\partial s$ map which, in the interesting region, is weaker by roughly a factor of 2 to 3 compared to the $\partial F_{\mathrm{xc}}/\partial s$ map of PBE (see Fig. 2). It also has negative areas which partially cancel the contributions from positive areas, even further undermining the significance of the $G_3^{\mathrm{QNA(Au)}}$ contribution. This is why Au, for instance, prefers such a choice of optimal parameters, since they lead to an LDA-like steep dE_{xc}/dw slope and thus a correct lattice constant.

B. Bulk moduli

Unlike in Refs. [27,34–36], our results find the MAE (MUE in Ref. [36]) of PBEsol is smaller than that of PBE. This is at least partly due to the use of ZPPE-corrected experimental bulk moduli. As PBEsol generally (except for Li in Table I) produces larger bulk moduli than PBE, ZPPE corrections favour PBEsol, since these corrections increase the values of experimental bulk moduli. On average (MEs and MREs in Table I), PBE produces bulk moduli that are too small and PBEsol bulk moduli that are too large, while QNA has no strong bias towards either overestimation or underestimation.

In terms of bulk modulus, the improvements offered by QNA approximation are very clear. In most cases such good optimal parameters can be found that MAE and MARE of QNA in Table I are less than a half of the MAE and MARE of PBEsol. For many of the heavier elements, however, PBEsol produces the most accurate bulk modulus. Ba seems to be a difficult case as the relative error of the QNA bulk modulus remains at 11%.

The value of the calculated bulk modulus of different functionals is mostly determined by the volume dependence of the total energy, which causes the error in the bulk modulus to be inversely related to the error in the lattice constant [37].

This is, for example, why LDA tends to overestimate bulk moduli while PBE underestimates them. There is, however, a secondary effect which becomes important within QNA when the value of the bulk modulus is tuned while keeping the volume fixed to its optimal value. This secondary effect is the contribution coming from the curvature $\partial^2 E_{\rm xc}/\partial w^2$ of the $E_{\rm xc}$ vs V curve. Increasing (decreasing) the negative curvature of the $E_{\rm xc}$ vs V curve while keeping the overall slope (difference between the end points) fixed moves points higher (lower) in energy near the equilibrium volume and makes the $E_{\rm tot}$ vs V curve shallower (deeper) thus giving smaller (higher) bulk modulus. The curvature arising from the interesting region is of the form

$$\frac{\partial^2 E_{\rm xc}^{\rm cvor}}{\partial w^2} = A(H_1 + H_2 + H_3 + H_4 + H_5 + H_6), \quad (9)$$

where the six contributors H_1–H_6 have been grouped in terms of the enhancement factor $F_{\rm xc}$ and its derivatives, and they are

$$H_1 = \int_{\rm cvor} F_{\rm xc}\left[\frac{4}{r_s^5}\frac{d^2 r_s}{dw^2} - \frac{20}{r_s^6}\left(\frac{dr_s}{dw}\right)^2\right] d^3r, \quad (10)$$

$$H_2 = \int_{\rm cvor} \frac{\partial F_{\rm xc}}{\partial r_s}\left[\frac{8}{r_s^5}\left(\frac{dr_s}{dw}\right)^2 - \frac{1}{r_s^4}\frac{d^2 r_s}{dw^2}\right] d^3r, \quad (11)$$

$$H_3 = \int_{\rm cvor} \frac{\partial F_{\rm xc}}{\partial s}\left[\frac{8}{r_s^5}\frac{dr_s}{dw}\frac{ds}{dw} - \frac{1}{r_s^4}\frac{d^2 s}{dw^2}\right] d^3r, \quad (12)$$

$$H_4 = -\int_{\rm cvor} \frac{\partial^2 F_{\rm xc}}{\partial s \partial r_s}\frac{2}{r_s^4}\frac{dr_s}{dw}\frac{ds}{dw} d^3r, \quad (13)$$

$$H_5 = -\int_{\rm cvor} \frac{\partial^2 F_{\rm xc}}{\partial r_s^2}\frac{1}{r_s^4}\left(\frac{dr_s}{dw}\right)^2 d^3r, \quad (14)$$

$$H_6 = -\int_{\rm cvor} \frac{\partial^2 F_{\rm xc}}{\partial s^2}\frac{1}{r_s^4}\left(\frac{ds}{dw}\right)^2 d^3r. \quad (15)$$

Similarly to Eq. (5), the biggest contribution comes from the negative H_1 term. The second most important terms are H_2, H_3, and H_6, while H_4 and H_5 most of the time yield practically negligible contributions, because the second partial derivatives of $F_{\rm xc}$ involving $\partial/\partial r_s$ generally tend to be small. $\partial F_{\rm xc}/\partial s$ and $\partial^2 F_{\rm xc}/\partial s^2$ terms are much more sensitive to the details of the functional than their r_s counterparts, making H_3 and H_6 contributions vary between high importance and insignificance depending on the actual case (see Table II). $d^2 r_s/dw^2$ and $d^2 s/dw^2$ seem to be of the same order of magnitude as each other as well as with dr_s/dw and ds/dw. For most elements tested the curvature becomes smaller in magnitude, which is to say the value of the bulk modulus increases as we move higher in β along the curve of fixed optimal volume in $\{\mu,\beta\}$ space. Figure 1 displays one such curve for V. The heaviest elements Pb and Au have the opposite behavior. Not as clear a trend has been observed with elements having small bulk modulus, such as Li, which could be due to numerical difficulties associated with very shallow $E_{\rm tot}$ vs V curves.

To better understand how these differences in curvatures as a function of optimal β come about, we have approximated the terms G_1–G_3 and H_1–H_6 by calculating them in the $\hat{z}$ direction inside the core-valence overlap region within the Wigner–Seitz cell at the QNA equilibrium volume for V and Au. The NSC approach has been used, which means that r_s, s and their first and second derivatives stay the same and only $F_{\rm xc}$ and its derivatives change between different sets of calculations.

TABLE II. Calculated values of G_1-G_3, $G_{\rm tot}$, H_1-H_6, and $H_{\rm tot}$ for V and Au using three different equivolume $\{\mu,\beta\}$ pairs.

	V, $a_0 = 3.024$ Å			Au, $a_0 = 4.068$ Å		
μ	0.1880	0.2995	0.2945	0.0168	0.0969	0.1250
β	0.0050	0.0500	0.1000	0.005	0.0500	0.1000
B_0 (GPa)	163	167	170	188	188	187
G_1	0.856	0.854	0.840	0.614	0.608	0.597
G_2	−0.016	−0.015	−0.013	−0.012	−0.011	−0.009
G_3	−0.078	−0.077	−0.066	−0.001	−0.003	−0.006
$G_{\rm tot}$	0.762	0.762	0.761	0.601	0.594	0.584
H_1	−2.159	−2.155	−2.118	−2.004	−1.985	−1.953
H_2	0.052	0.047	0.041	0.046	0.040	0.032
H_3	0.183	0.187	0.169	0.003	0.009	0.018
H_4	0.000	0.005	0.008	0.000	0.006	0.012
H_5	0.003	0.002	0.002	0.001	0.001	0.001
H_6	−0.036	−0.037	−0.051	−0.001	−0.029	−0.068
$H_{\rm tot}$	−1.957	−1.950	−1.948	−1.955	−1.958	−1.959

Table II shows results for three different pairs of optimal μ and β, yielding the same volume as in Table I. The sums $G_{\rm tot} = G_1 + G_2 + G_3$ and $H_{\rm tot} = H_1 + H_2 + H_3 + H_4 + H_5 + H_6$, respectively describing the slope and curvature of an $E_{\rm xc}$ vs V curve, are in decent agreement with the observable trends relating to calculated volumes and bulk moduli as μ and β are changed. $G_{\rm tot}$ stays nearly constant (except for Au in the high-β limit), as it should since all three pairs of μ and β give identical equilibrium volumes. $G_{\rm tot}$ also respects sequences $G_{\rm tot}^{\rm LDA} > G_{\rm tot}^{\rm PBEsol} > G_{\rm tot}^{\rm PBE} > G_{\rm tot}^{\rm QNA(V)}$ and $G_{\rm tot}^{\rm LDA} \approx G_{\rm tot}^{\rm QNA(Au)} > G_{\rm tot}^{\rm PBEsol} > G_{\rm tot}^{\rm PBE}$ (not shown), which agrees with the observed ordering of the lattice constants.

For V (Au) $H_{\rm tot}$ decreases (increases) in magnitude with increasing β, which agrees with the way bulk modulus evolves through increasing β. Despite H_1 being a major part of $H_{\rm tot}$, looking at H_1 alone is not enough to explain these trends. For Au all terms except H_5 have to be taken into account to make $H_{\rm tot}$ slowly increase in magnitude as β is increased.

C. Optimal parameters

Optimal parameters minimizing the combined error in lattice constant and bulk modulus for the selected elements are presented in Table III. They are also laid out graphically in $\{\mu,\beta\}$ space in Fig. 3. The best optimal values yielding nearly vanishing errors can generally be obtained in cases where either PBE or PBEsol tends to underestimate the lattice constant but overestimate bulk modulus, or vice versa. This feature enables efficient matching of the volume and bulk modulus errors, since increasing volume generally decreases the value of bulk modulus and vice versa. Note that while it is possible to completely minimize the error either in lattice constant or bulk modulus, it is much more difficult to completely minimize both errors at the same time. The presently employed PBE or PBEsol functional form is not flexible enough to allow for that.

TABLE III. Values of optimal parameters which minimize the combined error in lattice constant and bulk modulus [Eq. (2)] for the selected solids.

Solid	μ_{opt}	β_{opt}
Li (bcc)	0.087 8000	0.071 8111
Na (bcc)	0.096 0000	0.000 0010
K (bcc)	0.118 7816	0.047 2974
Rb (bcc)	0.122 0000	0.055 0631
Cs (bcc)	0.133 3000	0.018 0581
Ca (fcc)	0.150 0000	0.100 0000
Sr (fcc)	0.147 0000	0.005 0000
Ba (bcc)	0.195 0000	0.027 3746
Al (fcc)	0.114 7214	0.040 1048
Pb (fcc)	0.126 0000	0.100 0000
V (bcc)	0.188 0000	0.005 0000
Cr (bcc)	0.075 0000	0.000 2000
Fe (bcc)	0.148 5000	0.005 0000
Ni (fcc)	0.102 0000	0.005 0000
Cu (fcc)	0.079 5000	0.005 0000
Nb (bcc)	0.173 0000	0.100 0000
Mo (bcc)	0.160 0000	0.100 0000
Rh (fcc)	0.050 0000	0.005 0000
Pd (fcc)	0.141 5645	0.100 0000
Ag (fcc)	0.107 0000	0.035 3330
Ta (bcc)	0.145 0000	0.065 4408
W (bcc)	0.060 5000	0.005 0000
Ir (fcc)	0.025 0000	0.005 0000
Pt (fcc)	0.113 0000	0.056 1219
Au (fcc)	0.125 0000	0.100 0000

In light of the mean errors in Table I constructing a functional out of element-specific subfunctionals is one clear way of improving accuracy, while it has proven to be difficult to design an element independent GGA-level functional form that would have a consistent performance across the periodic table [10,27]. The difficulty lies in the fact that while some pair of elements assume fairly similar values of r_s and s in the core-valence overlap region, they might require very differently shaped $F_{\text{xc}}^{\text{opt}_q}(r_s,s)$ maps. As a result an element independent functional with only one $F_{\text{xc}}(r_s,s)$ map would have to be able to change its shape very rapidly and nontrivially as a function of r_s and s over relatively short distances.

For the sake of reducing computational time the optimization process was done using NSC-GGA, i.e., self-consistent calculations were performed at LDA level and gradient corrections were included in the total energies as perturbations. To test the validity of these NSC-derived optimal parameters in conjunction with a fully self-consistent method further SC-EMTO and FP-(L)APW + lo Elk calculations for Li, V, Fe, Cu, Nb, and Au were carried out. Results of these calculations along with the accompanying experimental values are presented in Table IV.

The differences between NSC-EMTO and SC-EMTO lattice parameters are very small. Bulk moduli show minor deviations with the ~ -4 GPa difference of Fe being the most notable. Similar observation concerning the discrepancy between the NSC and SC bulk moduli of Fe has been made in Ref. [18] where it was attributed to a connection between the

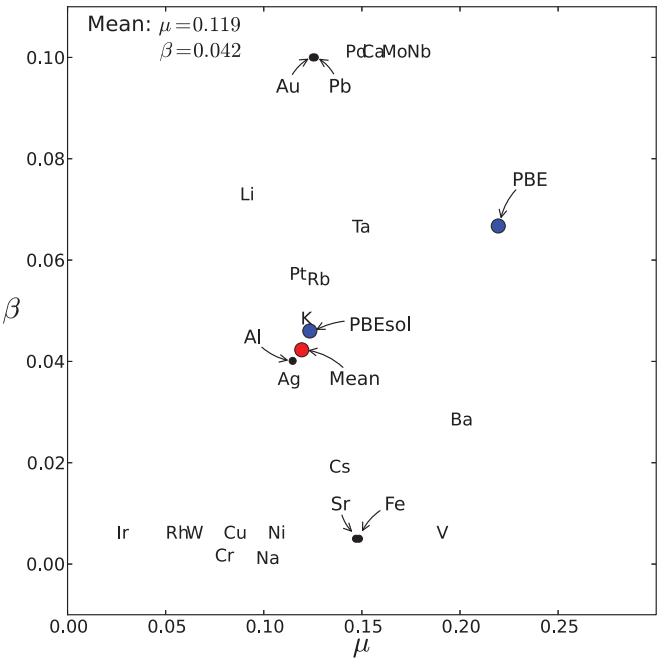

FIG. 3. (Color online) Optimal parameters for the selected monatomic solids. PBE and PBEsol points as well as the mean of the QNA optimal parameters are also drawn as annotated.

gradient effects and the nonspherical spin densities of Fe. In our case, however, the SC treatment increases the bulk modulus of Fe, while in Ref. [18] (all-electron FP-KKR) it decreased.

Elk results in general agree very well with the NSC-EMTO calculations and thus with the experimental values. For Au the Elk lattice parameter becomes too small and bulk modulus

TABLE IV. Self-consistent GGA lattice constants a_0 (in Å) and bulk moduli (in GPa) calculated with EMTO and Elk using PBE and QNA functionals for Li, V, Fe, Cu, Nb, and Au. QNA is using the optimal parameters from Table III. Δ_a (in Å $\times 10^{-3}$) and Δ_B (in GPa) indicate the difference compared to the NSC-EMTO results of Table I for QNA ("NSC − SC" or "NSC − Elk").

	EMTO					
	a_0			B_0		
Solid	QNA	PBE	Δ_a	QNA	PBE	Δ_B
Li (bcc)	3.442	3.433	2	13.5	14.0	0
V (bcc)	3.023	2.996	1	164	176	−1
Fe (bcc)	2.854	2.836	0	179	193	−4
Cu (fcc)	3.602	3.637	0	150	139	0
Nb (bcc)	3.286	3.308	2	165	160	2
Au (fcc)	4.069	4.177	−1	185	135	1
	Elk					
	a_0			B_0		
Solid	QNA	PBE	Δ_a	QNA	PBE	Δ_B
Li (bcc)	3.442	3.433	2	13.5	13.9	0
V (bcc)	3.027	3.002	−3	170	181	−7
Fe (bcc)	2.850	2.834	4	177	194	−2
Cu (fcc)	3.598	3.632	4	153	141	−3
Nb (bcc)	3.294	3.314	−6	176	169	−9
Au (fcc)	4.048	4.149		199	145	

too high, but this is mostly due to the inclusion of spin-orbit coupling, which was not present in the NSC-EMTO calculations. Elk bulk moduli show some differences. This is expected, since by comparing, for example, the results of Table I and Ref. [34] (PBE, EMTO) to the results in the supplementary material of Ref. [28] (PBE, WIEN2K) one can see that bulk moduli in Elk and in methods similar to Elk [FP-(L)APW+lo] tend to be higher than their EMTO counterparts for many of the $3d$, $4d$, and $5d$ metals. For solids such as Nb, for which QNA underestimates the bulk modulus, this is only beneficial. On the other hand, for solids with overestimated NSC-QNA bulk moduli the SC-QNA bulk modulus can be further overestimated depending on the employed computational method. Therefore, depending on the solid and the used computational method, it might be necessary to further optimize the values given in Table III to make them better suited for SC-QNA calculations. For example, optimal μ for Au should be increased from its value of 0.125 to compensate for the inclusion of spin-orbit coupling. Generally speaking, increasing μ will increase (decrease) the calculated lattice constant (bulk modulus) and vice versa, while increasing β tends to decrease (increase) the calculated lattice constant (bulk modulus) up to some element specific point, after which the trend is reversed (see Fig. 2 of Ref. [10]).

It is interesting to note how in Fig. 3 the mean value of the optimal parameters nearly coincides with the PBEsol parameters. If the restriction $\beta \leqslant 0.1$ were to be lifted to allow Ca, Nb, Mo, Pd, Au, and Pb (see Fig. 3 and Table III) to have even higher values of optimal β, the agreement between the mean and PBEsol parameters would be even more convincing. It is not, however, surprising that the mean should be closer to PBEsol parameters than those of PBE, since PBEsol was designed for solids, so perhaps the mean of the optimal parameters can thus be viewed as an alternative confirmation of the PBEsol parameters.

D. Applications

The performance of QNA scheme is tested on random $Fe_{1-x}V_x$ solid solution and ordered NiAl intermetallic compound having bcc and B2 structures, respectively. Previously, good performance for VW solid solution and CuAu ($L1_0$) and Cu_3Au ($L1_2$) intermetallic compounds has been reported [10]. Here FeV was treated using the NSC-GGA approach and coherent potential approximation [39,40] and for both FeV and NiAl optimal parameters from Table III were used. The experimental values are from Ref. [38] (FeV) and Ref. [27] (NiAl). For FeV the experimental values have not been corrected to 0 K (room temperature). The experimental values of NiAl are extrapolated to 0 K and the lattice constant includes ZPAEs but the bulk modulus does not include ZPPEs. The results are gathered in Table V. It is no surprise that PBE underestimates the lattice constant of FeV, since it does so for both of the constituents. This results in the PBE bulk modulus being too large, as well. QNA corrects for these errors, improving the description of both quantities. At high V concentrations QNA lattice constant starts to deviate from the experimental value, which is due to the fact that the optimal parameters of V were calculated using the 0 K ZPAE-corrected experimental value (3.024 Å) which is markedly smaller than the room temperature value of Table V (3.042 Å). 0 K corrections to the experimental values would significantly improve the accuracy at the V-rich end.

TABLE V. Lattice constants a_0 (in Å) and bulk moduli (in GPa) for bcc $Fe_{1-x}V_x$ and B2 NiAl calculated with EMTO using PBE and QNA functionals. QNA is using the optimal parameters from Table III. Experimental values from Ref. [38] (FeV, room temperature) and Ref. [27] (NiAl, 0 K) are also included.

EMTO						
	a_0			B_0		
Solid	QNA	PBE	Expt.	QNA	PBE	Expt.
NiAl (B2)	2.881	2.894	2.882	163	159	156
Fe (bcc)	2.854	2.838	2.858	175	189	170
$Fe_{75}V_{25}$ (bcc)	2.889	2.870	2.886	171	184	166
$Fe_{50}V_{50}$ (bcc)	2.919	2.897	2.914	169	183	161
$Fe_{25}V_{75}$ (bcc)	2.948	2.924	2.963	188	202	182
Fe_6V_{94} (bcc)	3.004	2.978	3.020	169	183	172
V (bcc)	3.024	2.998	3.042	163	177	163

The PBE lattice constant of NiAl is too large but the bulk modulus is reproduced quite accurately due to cancellation of errors. QNA on the other hand gives an accurate lattice constant at the expense of slightly overestimated bulk modulus. We would like to highlight that the optimal parameters of Al and Ni were determined for their equilibrium fcc structures whereas NiAl adopts a bcc-like B2 structure. Hence, our findings demonstrate that at ambient conditions the optimal parameters are not dependent on the crystal structure and chemical environment. However, they might be sensitive to extremely high pressure, which is a question to be investigated in the future.

IV. CONCLUSIONS

We have investigated the flexibility of the quasi-non-uniform xc approximation and have shown it to be able to significantly improve the description of lattice constants and bulk moduli over the currently used popular GGA functionals for a large set of metals and their alloys. QNA achieves this by applying local corrections separately in each core-valence overlap region of the system at hand. Designing a uniform, element-independent functional that would have a similar, consistent accuracy across the periodic table seems to be a rather difficult task. For any element tested, it is possible to completely minimize the error either in calculated volume or the bulk modulus but it is much more difficult to completely minimize both errors at the same time. The presently employed PBE functional form is not flexible enough to allow this.

ACKNOWLEDGMENTS

H.L. thanks Matti Ropo for providing comments and feedback. L.V. acknowledges the financial support from Swedish Research Council, the Swedish Steel Producers' Association, the European Research Council, and the Hungarian Scientific Research Fund (research project OTKA 84078 and 109570). The computer resources of the Finnish IT Center for Science (CSC) and the FGI project (Finland) are acknowledged.

[1] P. Hohenberg and W. Kohn, Phys. Rev. **136**, B864 (1964).
[2] W. Kohn and L. J. Sham, Phys. Rev. **140**, A1133 (1965).
[3] K. Burke, J. P. Perdew, and M. Ernzerhof, Int. J. Quantum Chem. **61**, 287 (1997).
[4] P. Bagno, O. Jepsen, and O. Gunnarsson, Phys. Rev. B **40**, 1997 (1989).
[5] D. J. Singh, W. E. Pickett, and H. Krakauer, Phys. Rev. B **43**, 11628 (1991).
[6] B. Barbiellini, E. G. Moroni, and T. Jarlborg, J. Phys.: Cond. Matter **2**, 7597 (1990).
[7] R. Armiento and A. E. Mattsson, Phys. Rev. B **66**, 165117 (2002).
[8] W. Kohn, Phys. Rev. Lett. **76**, 3168 (1996).
[9] J. P. Perdew, K. Burke, and M. Ernzerhof, Phys. Rev. Lett. **77**, 3865 (1996).
[10] H. Levämäki, M. P. J. Punkkinen, K. Kokko, and L. Vitos, Phys. Rev. B **86**, 201104 (2012).
[11] M. Fuchs, M. Bockstedte, E. Pehlke, and M. Scheffler, Phys. Rev. B **57**, 2134 (1998).
[12] P. Haas, F. Tran, P. Blaha, K. Schwarz, and R. Laskowski, Phys. Rev. B **80**, 195109 (2009).
[13] G. I. Csonka, J. P. Perdew, A. Ruzsinszky, P. H. T. Philipsen, S. Lebegue, J. Paier, O. A. Vydrov, and J. G. Angyan, Phys. Rev. B **79**, 155107 (2009).
[14] J. P. Perdew, A. Ruzsinszky, G. I. Csonka, O. A. Vydrov, G. E. Scuseria, L. A. Constantin, X. Zhou, and K. Burke, Phys. Rev. Lett. **100**, 136406 (2008).
[15] O. K. Andersen, O. Jepsen, and G. Krier, in *Lectures on Methods of Electronic Structure Calculation*, edited by V. Kumar, O. K. Andersen, and A. Mookerjee (World Scientific, Singapore, 1994), p. 63.
[16] L. Vitos, *Computational Quantum Mechanics for Materials Engineers: The EMTO Method and Applications, Engineering Materials and Processes Series* (Springer-Verlag, London, 2007).
[17] L. Vitos, Phys. Rev. B **64**, 014107 (2001); L. Vitos, I. A. Abrikosov, and B. Johansson, Phys. Rev. Lett. **87**, 156401 (2001).
[18] M. Asato, A. Settels, T. Hoshino, T. Asada, S. Blügel, R. Zeller, and P. H. Dederichs, Phys. Rev. B **60**, 5202 (1999).
[19] R. Hafner, D. Spisak, R. Lorenz, and J. Hafner, Phys. Rev. B **65**, 184432 (2002).
[20] A. E. Kissavos, L. Vitos, and I. A. Abrikosov, Phys. Rev. B **75**, 115117 (2007).
[21] A. B. Alchagirov, J. P. Perdew, J. C. Boettger, R. C. Albers, and C. Fiolhais, Phys. Rev. B **63**, 224115 (2001).
[22] http://elk.sourceforge.net/.
[23] W. M. Haynes, *CRC Handbook of Chemistry and Physics*, 94th ed. (CRC press, Boca Raton, 2013).
[24] V. N. Staroverov, G. E. Scuseria, J. Tao, and J. P. Perdew, Phys. Rev. B **69**, 075102 (2004).
[25] C. Kittel and P. McEuen, *Introduction to Solid State Physics* (Wiley, Hoboken, 2005).
[26] R. Gaudoin and W. M. C. Foulkes, Phys. Rev. B **66**, 052104 (2002).
[27] P. Haas, F. Tran, and P. Blaha, Phys. Rev. B **79**, 085104 (2009).
[28] P. Haas, F. Tran, P. Blaha, and K. Schwarz, Phys. Rev. B **83**, 205117 (2011).
[29] K. A. Gschneider Jr., in *Solid State Physics: Advances in Research and Applications*, edited by H. Ehrenreich and D. Turnbull (Academic, New York, 1964), Vol. 16, p. 276.
[30] D. I. Bolef, R. E. Smith, and J. G. Miller, Phys. Rev. B **3**, 4100 (1971).
[31] J. J. Adams, D. S. Agosta, R. G. Leisure, and H. Ledbetter, J. Appl. Phys. **100**, 113530 (2006).
[32] A. Dewaele, P. Loubeyre, and M. Mezouar, Phys. Rev. B **70**, 094112 (2004).
[33] A. E. Mattsson, R. Armiento, J. Paier, G. Kresse, J. M. Wills, and T. R. Mattsson, J. Chem. Phys. **128**, 084714 (2008).
[34] M. Ropo, K. Kokko, and L. Vitos, Phys. Rev. B **77**, 195445 (2008).
[35] P. Janthon, S. M. Kozlov, F. Vines, J. Limtrakul, and F. Illas, J. Chem. Theory Comput. **9**, 1631 (2013).
[36] F. Labat, E. Bremond, P. Cortona, and C. Adamo, J. Mol. Model. **19**, 2791 (2013).
[37] B. Grabowski, T. Hickel, and J. Neugebauer, Phys. Rev. B **76**, 024309 (2007).
[38] M. S. Lucas, J. A. Munoz, O. Delaire, N. D. Markovskiy, M. B. Stone, D. L. Abernathy, I. Halevy, L. Mauger, J. B. Keith, M. L. Winterrose, Y. Xiao, M. Lerche, and B. Fultz, Phys. Rev. B **82**, 144306 (2010).
[39] P. Soven, Phys. Rev. **156**, 809 (1967).
[40] B. L. Györffy, Phys. Rev. B **5**, 2382 (1972).